Proceedings of Global Power and Propulsion Society
ISSN-Nr: 2504-4400
GPPS Xi'an21
18th – 20th October, 2021
www.gpps.global

GPPS-TC-2021-0038

Quantification of Swirl Distortions Caused by S-shape Inlet Ducts

Zhenyu LI
School of Energy and Power Engineering
153079701@qq.com
Beijing, China

Xu DONG
Research Institute of Aero-engine
buaadongxu@buaa.edu.cn
Beijing, China

Dakun SUN
School of Energy and Power Engineering
sundk@buaa.edu.cn
Beijing, China

Xiaofeng SUN
School of Energy and Power Engineering
sunxf@buaa.edu.cn
Beijing, China

ABSTRACT

The S-shape inlet is generally the main reason for the occurrence of swirl inlet distortion that is seriously concerned by the manufactures of fighters. The non-uniform inlet combined with large-scale bulk swirl, small-scale tight-wound swirl, or both of them may greatly impact the performance of aero-engines. Focusing on the swirl patterns and the effects of swirl flow on the compression system, many attempts have been carried out. However, there is still no general and quantitative criterion for assessing the swirl pattern and intensity to serve the further performance or stability analysis. In this paper, a vorticity-based method was used to quantify the swirl inlet distortion caused by different S-inlet ducts. Three series of S-ducts with different offset distances and different lengths were designed. Numerical investigations on the intensity and form of swirl distortion were carried out to achieve quantitative results.

INTRODUCTION

The S-shape inlet has a significant advantage in reducing radar signature, and this kind of inlets have been widely used in the power system of modern aircrafts. However, the curvature of the S-duct brings a challenge to the flow control in the aircraft engine. The static pressure gradient and boundary layer separation in it usually cause some fluid dynamic phenomena at the aerodynamic interface plane (AIP), such as total pressure loss, total pressure distortion, static pressure distortion, and swirl distortion. These forms of distortions may change the performance and reduce the stall margin of compression system.

In order to study the influence of swirl distortion on compressor characteristics and stability boundary, different swirl distortion descriptors were proposed, such as *SC60*, *SI* series and τ_{87} series. Most of these descriptors are defined based on the swirl angle. The swirl distortion caused by S-ducts was also studied over the past decades. In the 1950s, there were basic researches on the internal flow in the elbow. In the 1970s, Bransod and Bradshaw investigated the fully developed flow in S-shaped ducts (Bransod and Bradshaw, 1972). In the 1980s, there were more experimental results and some numerical results proposed. Vakili et al. used surface oil flow visualization method and numerical method to study S-duct flow with an entrance Mach number of 0.6 (Vakili, 1983; Vakili, 1984). Guo and Seddon studied how the angle of attack influences the form of swirl distortion. It was found that counter-rotating vortices usually occur in low angle of attack, while bulk swirl usually occurs in high angle of attack (Guo and Seddon, 1982). Towne and Schum also proposed some numerical simulations (Towne and Schum, 1985). In the 1990s, Wellborn et al. used surface oil flow visualization to get the secondary flow at five different cross-sectional planes (Wellborn et al., 1992). Wendt and Reichert studied the effect of vortex ingestion on the secondary velocity field at AIP (Wendt and Reichert, 1994). In the 21st century, with the development of computer and numerical simulation, lots of numerical results were carried out. Although the steady and

unsteady simulations can achieve abundant flow details, relevant experiments are still necessary to verify the numerical results due to the complex secondary flow and boundary seperation. Recently, Zachos et al., Gil-Prieto et al. and McLelland et al. used stereoscopic particle image velocimetry (SPIV) to provide a clear view of the swirl flow field generated by two different S-shaped aero-engine intakes, and obtained the steady and unsteady flow characteristics inside these S-ducts (Zachos et al., 2016; Gil-Prieto et al., 2017; McLelland et al., 2020).

Among most of these investigations, the geometric construction of S-ducts is similar, though there may be differences in details. For S-ducts with circular cross sections, crucial geometric parameters include the offset (or height), the axial length (or length along the centerline), the area ratio (*AR*), the centerline function and the area distribution function. Typical S-inlets with relatively sufficient experimental research results are listed below.

1) Both the centerline function and the area distribution function are polynomial (Lee and Boedicker, 1985).

2) NASA Glenn Research Center's S-duct. Its centerline is created by two 30° circular arcs with the radius of 1.02 m.

The inlet diameter D_{in} is 0.2042m; the outlet diameter D_{out} is 0.2514m; the area ratio (*AR*) is 1.52. The flow inside this S-duct has been studied by Wellborn et al. (Wellborn et al., 1992; Wellborn et al., 1994). In addition, the low-offset S-duct studied by Zachos et al. (Zachos et al., 2016) is a scaled model of NASA Glenn Research Center's S-duct, with the inlet diameter D_{in} of 0.1216m and the outlet diameter D_{out} of 0.1500m.

3) The high-offset S-duct studied by Zachos et al. (Zachos et al., 2016). Its dimensionless axial length L/D_{in} is 4.95 and dimensionless offset e/D_{in} is 2.44, with the inlet diameter D_{in} of 0.1216m and the outlet diameter D_{out} of 0.1500m.

During the past half century, the development of advanced measurement technology and numerical simulation have made it easier to capture the main characteristics of flow inside the S-duct. The steady flow structure inside S-ducts has been studied sufficiently. However, the influence of geometric parameters on swirl distortion is rarely studied quantitatively. Sometimes designers of fighters need to estimate the swirl distortion caused by S-ducts quickly. This means that the swirl distortion pattern and intensity need to be calibrated using existing internal flow characteristics and geometric parameters.

The objective of this paper is to quantify the swirl inlet distortion caused by different S-ducts. This includes collection of some experimental and numerical results of S-ducts with different geometry characteristics. In the process of quantification, we mainly focus on the position and intensity of the cores of counter-rotating vortices at AIP. Based on the information of vortices above, some algorithms can be applied to reconstruct the secondary flow field at AIP. This has practical meaning in quickly estimating and reconstructing the swirl distortion pattern.

METHODOLOGY

Geometric characteristics of S-ducts

Figure 1 shows the definitions of some key geometric parameters of S-ducts. The S-ducts in this research belong to three different series. Details about the series A, B and C are listed in Table 1, 2 and 3, respectively. Some referenced experiments are listed in Table 4.

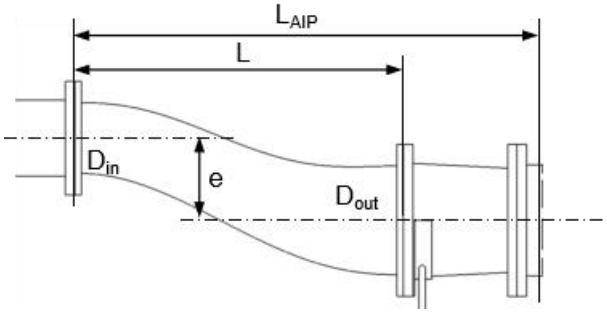

Figure 1 Key geometric parameters of S-ducts

Series A have medium offsets and large area ratios. Their geometry characteristics come from Liu's optimized ones (Liu et al., 2015). The centerline function and area distribution function are

$$\begin{aligned} \frac{y}{e} &= 3.34\left(\frac{x}{L}\right)^5 - 6.86\left(\frac{x}{L}\right)^4 + 1.69\left(\frac{x}{L}\right)^3 + 2.83\left(\frac{x}{L}\right)^2, \\ \frac{A(x)-A_{in}}{A_{out}-A_{in}} &= -7.9\left(\frac{x}{L}\right)^5 + 17\left(\frac{x}{L}\right)^4 - 12.3\left(\frac{x}{L}\right)^3 + 4.2\left(\frac{x}{L}\right)^2, \end{aligned} \tag{1}$$

where e is the offset; L is the axial length.

Series B have medium area ratios and different offset levels. The main purpose of series B is to investigate the influence of the offset on swirl distortion intensity. The centerline function and the area distribution function are

$$\frac{y}{e}=3\left(\frac{x}{L}\right)^4-8\left(\frac{x}{L}\right)^3+6\left(\frac{x}{L}\right)^2,$$
$$\frac{A(x)-A_{in}}{A_{out}-A_{in}}=3\left(\frac{x}{L}\right)^4-8\left(\frac{x}{L}\right)^3+6\left(\frac{x}{L}\right)^2, \quad (2)$$

where e is the offset; L is the axial length (Lee and Boedicker, 1985).

Series C are the same as NASA Glenn Research Center's S-duct. This series is mainly used to compare with the experiment results in Table 4.

Compared with the inlet Mach number, the AIP location is a more dominant non-geometric factor. It is limited to L_{AIP}/L = 1.40 ~ 1.60, where L_{AIP} is the axial distance between the entrance plane of the S-duct and the AIP.

Table 1 S-ducts of Series A

Simulations	*Ma*	e/D_{in}	L/D_{in}	*AR*	L_{AIP}/L	Centerline	Area Distribution
A1	0.18	0.8	4	2.10 (=1.45^2)	1.70		
A2	0.18	0.8	4	2.56 (=1.60^2)	1.70		
A3	0.18	0.8	5	1.69 (=1.30^2)	1.56		
A4	0.18	0.8	5	2.56	1.56		
A5	0.18	0.8	6	1.69	1.46		
A6	0.18	0.8	6	2.10	1.46		
A7	0.18	0.8	6	2.56	1.46		
A8	0.18	1.3	4	2.56	1.46		
A9	0.18	1.3	5	2.10	1.56		
A10	0.18	1.3	5	2.56	1.56	Equation (1)	Equation (1)
A11	0.18	1.3	6	1.69	1.46		
A12	0.18	1.3	6	2.10	1.46		
A13	0.18	1.3	6	2.56	1.46		
A14	0.18	1.8	6	1.69	1.46		
A15	0.18	0.9	5	2.10	1.56		
A16	0.18	1.0	5	2.10	1.56		
A17	0.18	1.1	5	2.10	1.56		
A18	0.18	1.2	5	2.10	1.56		
A19	0.18	1.2	6	2.56	1.46		

Table 2 S-ducts of Series B

Simulations	*Ma*	e/D_{in}	L/D_{in}	*AR*	L_{AIP}/L	Centerline	Area Distribution
B1	0.18	1.3	5	1.52 (=1.23^2)	1.50		
B2	0.18	1.3	6	1.52	1.50		
B3	0.18	1.0	5	1.52	1.50		
B4	0.18	1.7	5	1.52	1.50	Equation (2)	Equation (2)
B5	0.18	2.0	5	1.52	1.50		
B6	0.18	2.4	5	1.52	1.50		
B7	0.18	1.3	5	1.32 (=1.15^2)	1.50		
B8	0.18	1.3	5	1.69 (=1.30^2)	1.50		

Table 3 S-ducts of Series C

Simulations	*Ma*	e/D_{in}	L/D_{in}	*AR*	L_{AIP}/L	Centerline	Area Distribution
C1	0.20	1.34	5	1.52 (=1.23^2)	1.10		
C2	0.27	1.34	5	1.52	1.10	(Wellborn et	(Wellborn et
C3	0.20	1.34	5	1.52	1.50	al., 1992)	al., 1992)
C4	0.27	1.34	5	1.52	1.50		

Table 4 S-ducts of Experiments

Experiments	*Ma*	e/D_{in}	L/D_{in}	*AR*	L_{AIP}/L	Centerline	Area Distribution
E1 (Fiola and Ramesh, 2015)	0.6	1.34	5.00	1.231	1.10	The same as series C	The same as series C
E2 (Garnier et al., 2012)	-	2.44	4.95	1.231	-	-	-
E3 (Zachos et al., 2016)	0.27	1.34	5.00	1.231	1.10	The same as series C	The same as series C
E4 (Zachos et al., 2016)	0.6	1.34	5.00	1.231	1.10	The same as series C	The same as series C
E5 (Zachos et al., 2016)	0.27	2.44	4.95	1.231	1.10	-	-
E6 (Zachos et al., 2016)	0.6	2.44	4.95	1.231	1.10	-	-
E7 (Gil-Preito et al., 2020)	0.27	2.44	4.95	1.231	-	-	-

Grid Generation and Numerical Simulation Settings

Structured meshes were built using the ANSYS ICEM Meshing commercial software. The first layer of the boundary grid thickness was 5e-6 m to ensure $y+$ was approximately 1.

The Reynolds-averaged Navier-Stokes equations (RANS) were solved using the commercial software CFX. SSG Reynolds stress turbulence model was used because of the highly curved streamlines. The static temperature at the inlet was set to be 288 K; the static pressure at the outlet was set to be 101325 Pa; the walls were set to be no slip walls, smooth and adiabatic. The convergence criterion for the residue was set to be 5e-6.

Quantification Method of Swirl Distortion

The definition of most swirl distortion descriptors are based on the swirl angle. It may not applicable to flow with a wide axial velocity range, especially to flow with large boundary separation and backflow region at AIP. The streamline of secondary flow at AIP is another method to identify the swirl pattern directly, but it is usually rough and not specific. Since the swirl distortion caused by S-ducts is closely related to the viscous zone near the boundary layer, vortex-identification methods may be appropriate in describing the form and intensity. Some classic approaches in the field of vortex-identification methods include Q criterion, λ_2 criterion and vorticity criterion (Brrenden, 2017). The maximum of axial vorticity component is used here to quantify the intensity of swirl distortion, and the position of the maximum point is used to quantify the form of swirl distortion. Compared with Q criterion, its simple definition means it is easier to reconstruct the secondary flow field at AIP, and it has been verified that the results of vortex positions are almost the same as the results using Q criterion.

The swirl distortion of different S-ducts were analyzed based on the method above. Figure 2 illustrates the calibration in the vorticity field at AIP.

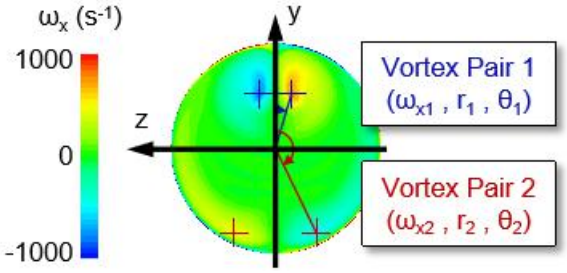

Figure 2 Calibration of vortices at AIP using vorticity

RESULTS AND DISCUSSION

Verification of the Numerical Results

The grid independence of case A9 and B1 was verified using total pressure recovery coefficient σ, as shown in Figure 3. The numerical result of case C2 was compared with experiment E3 by Zachos et al. (Zachos et al., 2016), as shown in Figure 4 and Figure 5. In Figure 4, parameter u_{ref} is the average axial velocity at AIP. In Figure 5, parameter u_θ is the circumferential component of secondary flow velocity.

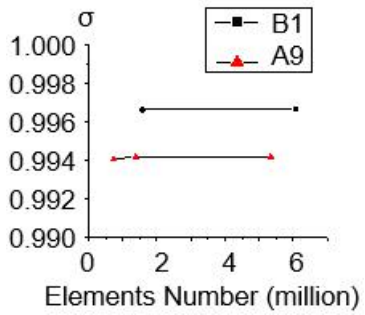

Figure 3 Grid independence verification

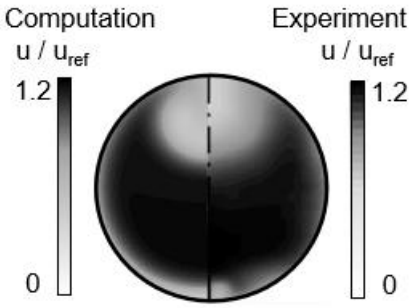

Figure 4
Axial velocity verification

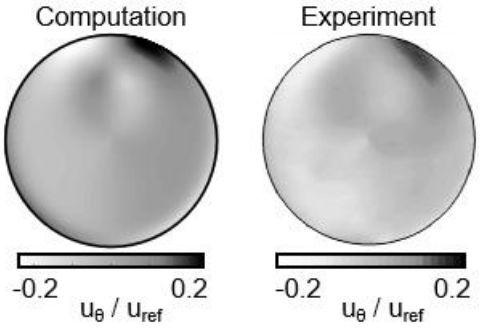

Figure 5
Circumferential velocity verification

Numerical Results and Quantification of Swirl Distortion

Figure 6 shows the axial vorticity component fields of different cases from series A and B at AIP. According to Figure 6, the offset influences the swirl distortion form significantly, compared with the length and the *AR*. Although most cases have two pairs of counter-rotating vortices at AIP, it is worth noting that if the offset is too low (especially when $e/D_{in} < 1.1$), there may only be one pair of vortices due to the low vorticity level. This phenomenon occurs in case A1~A7 and A15~A16. In addition, when the offset increases, the position of vortex pair 1 (see Figure 2) gradually moves to the center of the duct, while the position of vortex pair 2 (see Figure 2) slowly moves to the bottom.

Qualitatively, the influence of the offset, length and *AR* on the intensity of swirl distortion can be summarized as below: Increasing the offset or reducing the length of S-ducts can both increase the swirl distortion intensity by increasing the curvature of the centerline. Increasing the *AR* tends to reduce the swirl distortion intensity generally, which may due to the decrease of the velocity amplitude at AIP. It should be noted that the swirl distortion intensity here is defined using the axial vorticity component rather than the swirl angle.

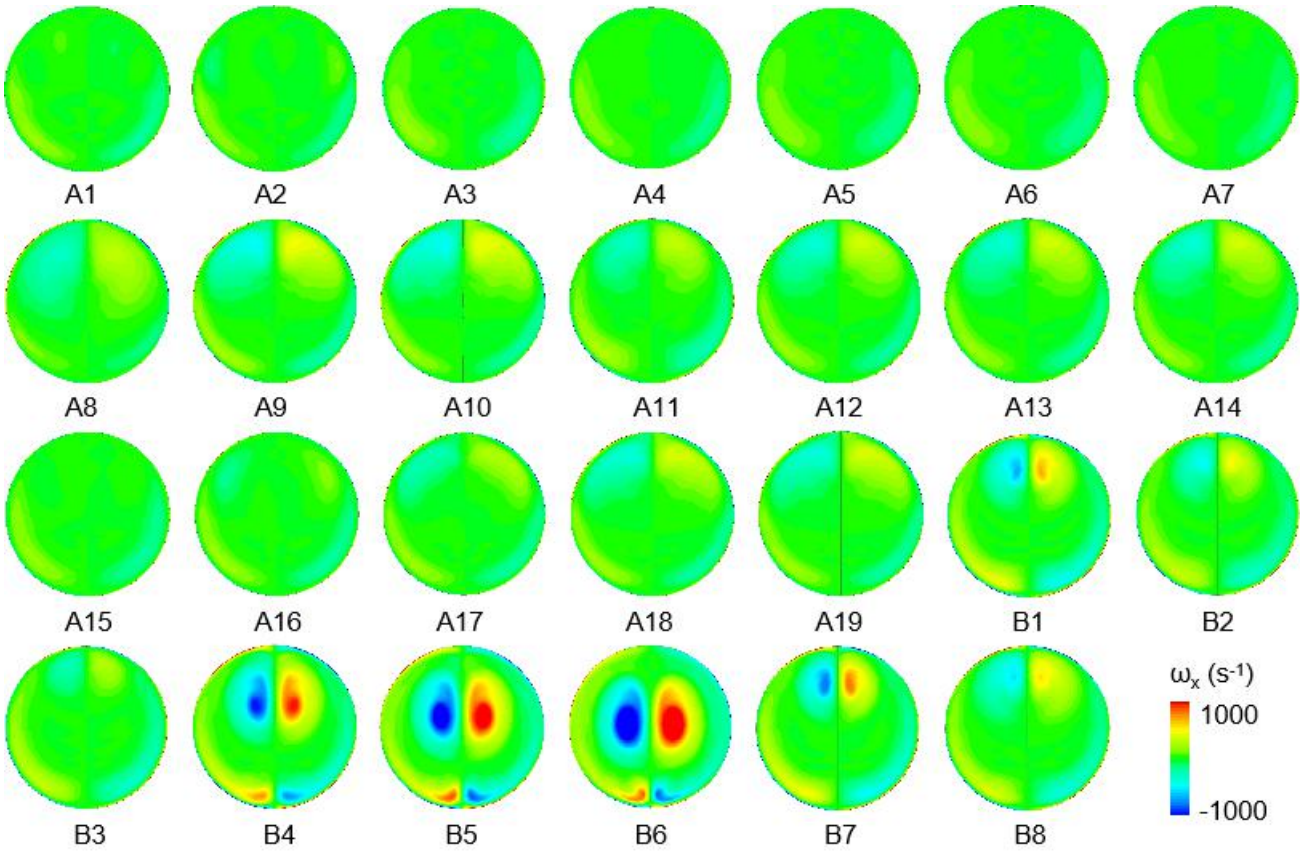

Figure 6 AIP vorticity fields of series A and B

Based on the qualitative results above, we attempted to quantify the swirl distortion caused by different S-ducts using AR and another parameter that is related to the curvature. The ratio e/L was found to be relatively reasonable to characterize the curvature of the centerline and normal static pressure gradient. The calibration results of vortices using these geometric parameters are presented in Figure 7. Figure 7a, 7b and 7c show the maximum vorticity, radial position and circumferential position of vortex pair 1 (see Figure 2), respectively; Figure 7d, 7e and 7f show the maximum vorticity, radial position and circumferential position of vortex pair 2 (see Figure 2). This calibration is roughly applicable in the following situations: the inlet Mach number Ma = 0.1 ~ 0.3; the offset e = 0.8 ~ 2.4 D_{in}; the axial length L = 4 ~ 6 D_{in}; the area ratio AR = 1.3 ~ 2.6; the location of AIP L_{AIP} = 1.3 ~ 1.5 L. The information shown in Figure 7 can help to quickly estimate the overall swirl distortion and secondary flow pattern of AIP.

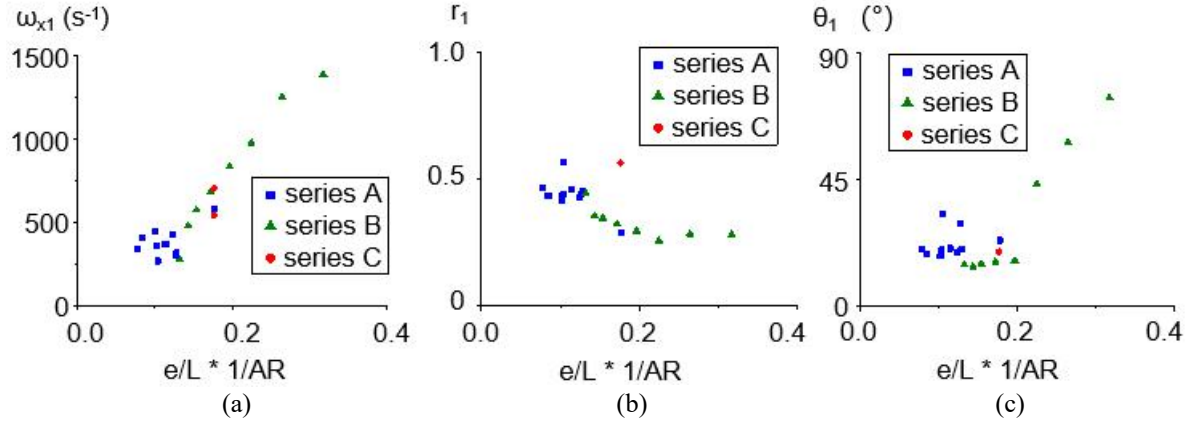

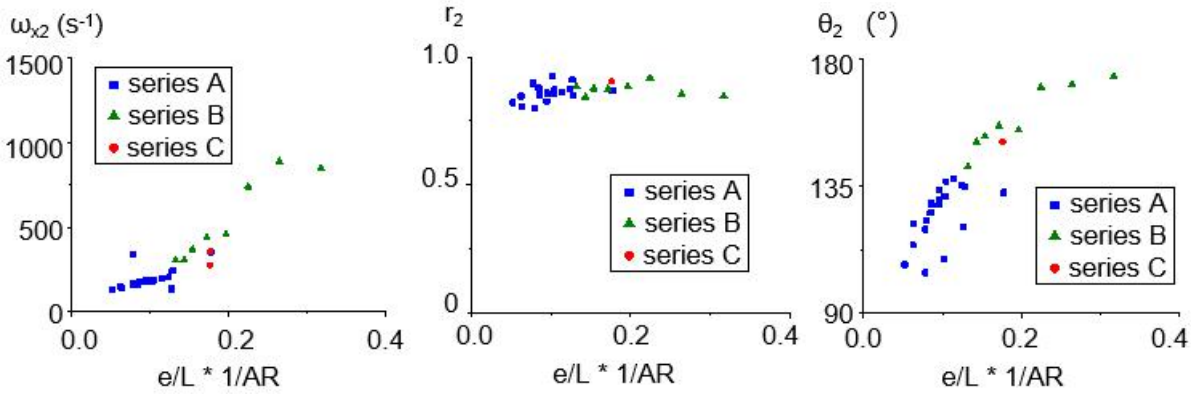

(d) (e) (f)

Figure 7 Calibration results of vortices using geometric parameters

CONCLUSIONS

The purpose of this work is to quantify the swirl inlet distortion caused by different sizes of S-ducts. To this aim, three series of S-ducts with different geometric characters were designed. Numerical investigations on the intensity and form of swirl distortion were carried out. The mesh independence was verified, and some numerical results were compared with referenced SPIV results.

The swirl distortion caused by S-ducts was calibrated by axial vorticity component. Among all the geometric parameters, the offset has an essential effect on swirl distortion form, while the axial length and the area ratio only have a modest effect on it. The offset and area ratio both have influences on swirl distortion intensity.

Qualitatively, the offset is positively correlated with swirl distortion intensity, while the area ratio and the axial length are negatively correlated with swirl distortion intensity. The intensity here was defined by vorticity. Quantitatively, the positions and the intensity of the two counter-rotating vortices at AIP is roughly related to the geometric parameter $e/(L*AR)$. The application scope of the association is as follows: the inlet Mach number Ma ranges from 0.1 to 0.3; the offset e ranges from 0.8 D_{in} to 2.4 D_{in}; the axial length L ranges from 4 D_{in} to 6 D_{in}; the area ratio AR ranges from 1.3 to 2.6; the location of AIP L_{AIP} ranges from 1.3 L to 1.5 L.

Some future work will attempt to broaden the application scope, including taking inlet Mach number and the location of AIP into consideration. Other classic vortex identification approaches can be used to help quantify the swirl distortion. The evolution and mechanism of swirl distortion in S-ducts also need to be investigated to improve the definition of the geometric parameter in quantifying the distortion pattern.

NOMENCLATURE

AIP	Aerodynamic interface plane
AR	Area ratio, $AR = (D_{out}/D_{in})^2$
D_{in}	The diameter of cross section at the entrance of the S-duct
D_{out}	The diameter of cross section at the exit of the S-duct
E	Offset
L	Axial length
L_{AIP}	The axial distance between the entrance plane of the S-duct and AIP
Ma	Mach number
r_1	The relative radius of vortex pair 1
r_2	The relative radius of vortex pair 2
R_{in}	The Radius of cross section at the entrance of the S-duct
R_{out}	The Radius of cross section at the exit of the S-duct
u	Axial velocity
u_{ref}	Average axial velocity at AIP
u_θ	The circumferential component of secondary flow velocity.
x	Axial position
y	The position of the offset direction
σ	Total pressure recovery coefficient
θ_1	The angle of vortex pair 1

θ_2	The angle of vortex pair 2
ω_{x1}	The vorticity component in x direction of vortex pair 1
ω_{x2}	The vorticity component in x direction of vortex pair 2

ACKNOWLEDGMENTS

The research presented here is supported by National Natural Science Foundation of China (Nos. 51906004, 51822601 and 51790514) and National Science and Technology Major Project (2017-II-0005-0018).

REFERENCES

Bansod, P., and Bradshaw, P. (1972). The Flow in S-shaped Ducts. *Aeronautical Quarterly*, 23(2), pp.131-140.

Brrenden, E. (2017). Review of Vortex Identification Methods. *55th AIAA Aerospace Sciences Meeting*. AIAA 2017-0989.

Fiola, C., and Agarwal, R. K. (2015). Simulation of Secondary and Separated Flow in Diffusing S Ducts. *Journal of Propulsion and Power*, 31(1), pp. 180-191.

Garnier, E., Leplat, M., Monnier, J. C., and Delva, J. (2012). Flow Control by Pulsed Jet in a Highly Bended S-Duct. *6th AIAA Flow Control Conference*. AIAA 2012-3250.

Gil Prieto, D., MacManus, D. G., Zachos, P., Tanguy, G., Wilson, F., and Chiereghin, N. (2017). Delayed Detached-Eddy Simulation and Particle Image Velocimetry Investigation of S-Duct Flow Distortion. *AIAA Journal*, 55(6), pp.1893-1908.

Guo, R., and Seddon, J. (1982). An Investigation of the Swirl in an S-Duct. *Aeronautical Quarterly*, 33(1), pp.25-58.

Lee, C., and Boedicker, C. (1985). Subsonic Diffuser Design and Performance for Advanced Fighter Aircraft. *Aircraft Design Systems and Operations Meeting*. AIAA 1985-3073.

Liu, L., Song, Y., Chen, H., Chen, F. (2015). Investigation on Effect of S-shaped Inlet Optimization to Internal Flow Characteristic and Aerodynamic Performance. *Journal of Engineering Thermophysics*, 36(1), pp. 50-54 (in Chinese).

McLelland, G., MacManus, D. G., Zachos, P., Gil Prieto, D., and Migliorini M. (2020). Influence of Upstream Total Pressure Profiles on S-Duct Intake Flow Distortion. *Journal of Propulsion and Power, 36(3)*, pp. 346-356.

Towne, C., and Schum, E. (1985). Application of Computational Fluid Dynamics to Complex Inlet Ducts. *21st Joint Propulsion Conference*. AIAA 1985-1213.

Vakili, A., Wu, J., Hingst, W., and Towne, C. (1984). Comparison of Experimental and Computational Compressible Flow in an S-Duct. *AIAA 22nd Aerospace Sciences Meeting*. AIAA 1984-33.

Vakili, A., Wu, J., Liver, P., and Bhat, M. (1983). Measurements of Compressible Secondary Flow in a Circular S-Duct. *AIAA 16th Fluid and Plasma Dynamics Conference*. AIAA 1983-1739.

Wellborn, S. R., Reichert, B. A., and Okiishi, T. H. (1992). An Experimental Investigation of the Flow in a Diffusing S-Duct. *28th Joint Propulsion Conference and Exhibit*. AIAA 1992-3622.

Wellborn, S. R., Reichert, B. A., and Okiishi, T. H. (1994). Study of the Compressible Flow in a Diffusing S-Duct. *Journal of Propulsion and Power*, 10(5), pp. 668–675.

Wendt, B., and Reichert, B. (1994). The Effects of Vortex Ingestion on the Flow in a Diffusing S-Duct. *30th Joint Propulsion Conference and Exhibit*. AIAA 1994-2811.

Zachos, P., MacManus, D. G., Gil Prieto, D., and Chiereghin N. (2016). Flow Distortion Measurements in Convoluted Aeroengine Intakes. *AIAA Journal*, 54(9), pp.2819-2832.